

Bayesian Implications for the Primordial Black Holes from NANOGrav's Pulsar-Timing Data Using the Scalar-Induced Gravitational Waves

Zhi-Chao Zhao ^{1,†}  and Sai Wang ^{2,3,*} 

¹ Department of Applied Physics, College of Science, China Agricultural University, Qinghua East Road, Beijing 100083, China; zhaozc@cau.edu.cn

² Theoretical Physics Division, Institute of High Energy Physics, Chinese Academy of Sciences, Beijing 100049, China

³ School of Physical Sciences, University of Chinese Academy of Sciences, Beijing 100049, China

* Correspondence: wangsai@ihep.ac.cn

† These authors contributed equally to this work.

Abstract: Assuming that the common-spectrum process in the NANOGrav 12.5-year dataset has an origin of scalar-induced gravitational waves, we study the enhancement of primordial curvature perturbations and the mass function of primordial black holes, by performing the Bayesian parameter inference for the first time. We obtain lower limits on the spectral amplitude, i.e., $\mathcal{A} \gtrsim 10^{-2}$ at 95% confidence level, when assuming the power spectrum of primordial curvature perturbations to follow a log-normal distribution function with width σ . In the case of $\sigma \rightarrow 0$, we find that the primordial black holes with $2 \times 10^{-4} - 10^{-2}$ solar mass are allowed to compose at least a fraction 10^{-6} of dark matter. Such a mass range is shifted to more massive regimes for larger values of σ , e.g., to a regime of $4 \times 10^{-3} - 0.2$ solar mass in the case of $\sigma = 1$. We expect the planned gravitational-wave experiments to have their best sensitivity to \mathcal{A} in the range of 10^{-4} to 10^{-7} , depending on the experimental setups. With this level of sensitivity, we can search for primordial black holes throughout the entire parameter space, especially in the mass range of 10^{-16} to 10^{-11} solar masses, where they could account for all dark matter. In addition, the importance of multi-band detector networks is emphasized to accomplish our theoretical expectation.

Keywords: Primordial black hole; Scalar-induced gravitational waves; Bayesian parameter inference; Pulsar-Timing data analysis

1. Introduction

It is well-known that the primordial black holes (PBHs) could be produced by gravitational collapses of the enhanced primordial curvature perturbations on small scales [1]. The mass function of PBHs is determined by the power spectrum of primordial curvature perturbations [2–4]. To produce a sizeable quantity of PBHs, the scalar spectral amplitude should conquer a critical magnitude ~ 0.1 [5], which is about eight orders of magnitudes larger than the spectral amplitude on large scales. On the other hand, the dynamics of cosmic inflation [6–8] is one of the greatest puzzles of cosmology to be uncovered. In particular, the small-scale primordial curvature perturbations were generated by quantum fluctuations at the late-time stage of inflation. Their power spectrum encodes characteristic information about the late-time dynamics of inflation, which could be different from that of the early-time one measured precisely with experiments on cosmic microwave background (CMB) [9,10] and large-scale structure (LSS) [11,12]. Therefore, we can gain more information about cosmic inflation by investigating the PBHs.

The scenario of PBHs can also be a reasonable candidate of dark matter, or compose a part of the latter [13,14]. The mass function of PBHs is defined as a ratio between the energy density fractions of PBHs and dark matter. Extensive studies have shown observational constraints on



Citation: Zhao, Z.-C.; Wang, S.

Bayesian Implications for the Primordial Black Holes from NANOGrav's Pulsar-Timing Data Using the Scalar-Induced Gravitational Waves. *Preprints* 2023, 1, 0. <https://doi.org/>

Academic Editor:



Copyright: © 2023 by the authors. Licensee MDPI, Basel, Switzerland. This article is an open access article distributed under the terms and conditions of the Creative Commons Attribution (CC BY) license (<https://creativecommons.org/licenses/by/4.0/>).

the mass function of PBHs (e.g., see reviews in Refs. [15,16]). In addition, the scenario of PBHs was suggested to interpret the formation mechanism of supermassive black holes (SMBHs) [17] and the events of compact binary coalescences [18–25], which emitted the gravitational waves (GWs) observed by the Advanced LIGO, Virgo and KAGRA detectors [26–28].

Accompanied by the formation process of PBHs, the scalar induced gravitational waves (SIGWs) [29–32] were inevitably produced by the enhanced primordial curvature perturbations. Specifically, they were produced through nonlinear couplings of tensor-scalar-scalar modes in the very early cosmos. Given the power spectrum of primordial curvature perturbations, a semi-analytic formula was provided to compute the energy density fraction spectrum of SIGWs [33,34]. It has been widely used to investigate the mass function of PBHs in the literature.

In this work, we will investigate the mass function of PBHs, as well as the power spectrum of primordial curvature perturbations, by analyzing a 12.5-year dataset from North American Nanohertz Observatory for Gravitational Waves (NANOGrav)¹ [35]. Strong evidence of a stochastic common-spectrum process was reported by NANOGrav Collaboration. If this signal has an origin of SIGWs, we can straightforwardly obtain constraints on the power spectrum of primordial curvature perturbations. Since the latter can collapse to form the PBHs due to gravity, we therefore obtain corresponding constraints on the mass function of PBHs. In fact, the scenario of PBHs with different masses has been suggested to interpret such a signal (see, e.g., Refs. [36–41]). However, there is still lack of systematic Bayesian parameter inferences, which will be performed for the first time in this paper.

The rest of the paper is arranged as follows. We briefly review the theory of SIGWs in Section 2. By performing Bayesian analysis, we obtain the NANOGrav constraints on the enhancement of primordial curvature perturbations in Section 3. Correspondingly, we demonstrate the physical implications for the mass function of PBHs in Section 4. We forecast the sensitivity curves of ongoing and planned gravitational-wave detectors in Section 5. The conclusion and discussion are shown in Section 6.

2. Theory of Scalar-Induced Gravitational Waves

As previously shown [33,34], there is a lengthy and tedious derivation process to obtain a semi-analytic formula for the energy density fraction spectrum of SIGWs in the early cosmos. Therefore, we summarize some theoretical results that would be essential to our data analysis. The energy density fraction spectrum of GWs is defined as $\Omega_{\text{GW}}(k) = \rho_{\text{GW}}(k)/\rho_c$, where k denotes the GW wavenumber, ρ_c is the critical energy density of the cosmos, and $\int \rho_{\text{GW}}(k) d \ln k$ denotes the total energy density of GWs. The SIGWs in the subhorizon have the energy density spectrum as $\rho_{\text{GW}} \sim \langle \overline{h_{ij,l} h_{ij,l}} \rangle$ [42], where the overbar stands for the oscillation average and the angle brackets defines the power spectrum. The strain of SIGWs, as the second-order tensor perturbations produced by the linear scalar perturbations, can be roughly expressed as $h \sim \phi^2$, where ϕ denotes the linear scalar perturbation. If considering the Gaussian scalar perturbations, we obtain $\rho_{\text{GW}} \sim \langle \phi^4 \rangle \sim \langle \phi^2 \rangle \langle \phi^2 \rangle$, where $\langle \phi^2 \rangle$ is determined by the initial value and transfer function of ϕ . Therefore, following Equation (14) of Ref. [33], the energy density fraction spectrum of SIGWs in the radiation-dominated cosmos is given as

$$\Omega_{\text{GW}}(k) = \int_0^\infty dv \int_{|1-v|}^{|1+v|} du F(v,u) \mathcal{P}_{\mathcal{R}}(vk) \mathcal{P}_{\mathcal{R}}(uk), \quad (1)$$

where $\mathcal{P}_{\mathcal{R}}(uk)$ (and $\mathcal{P}_{\mathcal{R}}(vk)$) is power spectrum of primordial curvature perturbations at wavenumber uk (and vk) with u (and v) being a dimensionless variable, and $F(v,u)$ is a functional of the scalar transfer function describing the post-inflationary evolution of ϕ and can be simplified as

$$\begin{aligned}
F(v, u) &= \frac{3}{2^{10} v^8 u^8} \left[4v^2 - (v^2 - u^2 + 1)^2 \right]^2 (v^2 + u^2 - 3)^2 \\
&\quad \times \left\{ \left[(v^2 + u^2 - 3) \ln \left(\left| \frac{3 - (v+u)^2}{3 - (v-u)^2} \right| \right) - 4vu \right]^2 \right. \\
&\quad \left. + \pi^2 (v^2 + u^2 - 3)^2 \Theta(v + u - \sqrt{3}) \right\}. \tag{2}
\end{aligned}$$

Due to a lack of direct measurements, the nature of primordial curvature perturbations on small scales remains unknown, compared with that on the largest scales measured by the cosmic microwave background. For computational simplicity, we take two concrete expressions of $\mathcal{P}_{\mathcal{R}}(k)$, which are frequently adopted in the literature (e.g., Refs. [33,43–46]), as follows

$$\mathcal{P}_{\mathcal{R}}(k) = \mathcal{A} \delta \left(\ln \frac{k}{k_*} \right), \tag{3}$$

$$\mathcal{P}_{\mathcal{R}}(k) = \frac{\mathcal{A}}{\sqrt{2\pi}\sigma} \exp \left(-\frac{\ln^2(k/k_*)}{2\sigma^2} \right), \tag{4}$$

where \mathcal{A} is an amplitude, σ is a standard variance, and k_* is a pivot wavenumber. We can relate the wavenumber with the frequency, i.e., $k = 2\pi f$ and $k_* = 2\pi f_*$. During the process of parameter inferences, both \mathcal{A} and f_* are independent parameters. However, we will not let σ be independent, even though different values of σ would alter our results. In fact, it is challenging to explore the full parameter space of σ based on the current dataset. Therefore, we let $\sigma = 1$ for simplicity in this work. We can test the robustness of our conclusions by comparing the results obtained when taking two different values of σ . In particular, we will compare the results from Equations (3) and (4). We leave this point to be demonstrated further in the following sections.

In Figure 1, we show the energy density fraction spectrum of SIGWs, which is normalized with \mathcal{A}^2 . For comparison, we show the results when taking different versions of σ . Equation (3) can be viewed as a limit of Equation (4) when $\sigma \rightarrow 0$. In the regime of $f \ll f_*$, the choice of $\sigma \rightarrow 0$ displays the highest spectral amplitude than non-vanishing choices of σ . This implies that in such a case, we can obtain the best sensitivity on measurements of \mathcal{A} for a given GW experiment. Correspondingly, we can obtain the strictest constraints on the mass function of PBHs. We will demonstrate these points in the following sections.

Once the early-universe quantity $\Omega_{\text{GW}}(k)$ is given in Equation (1), we have the energy density fraction spectrum of SIGWs in the present cosmos to be [43]

$$\Omega_{\text{GW},0}(f) = \Omega_{\text{r},0} \left[\frac{g_{*,\rho}(T)}{g_{*,\rho}(T_{\text{eq}})} \right] \left[\frac{g_{*,s}(T_{\text{eq}})}{g_{*,s}(T)} \right]^{\frac{4}{3}} \Omega_{\text{GW}}(k), \tag{5}$$

where $\Omega_{\text{r},0}$ is the present energy density fraction of radiations, and the subscript eq stands for cosmological quantities at the epoch of matter-radiation equality. Here, we have taken into account contributions from the effective relativistic degrees of the cosmos, i.e., $g_{*,\rho}$ and $g_{*,s}$, as functions of f by interpolating their tabulated data in terms of cosmic temperature T in Ref. [47]² as well as by considering a relation between T and f in Wang et al. [43], i.e.,

$$\frac{f}{\text{nHz}} = 26.5 \left(\frac{T}{\text{GeV}} \right) \left[\frac{g_{*,\rho}(T)}{106.75} \right]^{\frac{1}{2}} \left[\frac{g_{*,s}(T)}{106.75} \right]^{-\frac{1}{3}}. \tag{6}$$

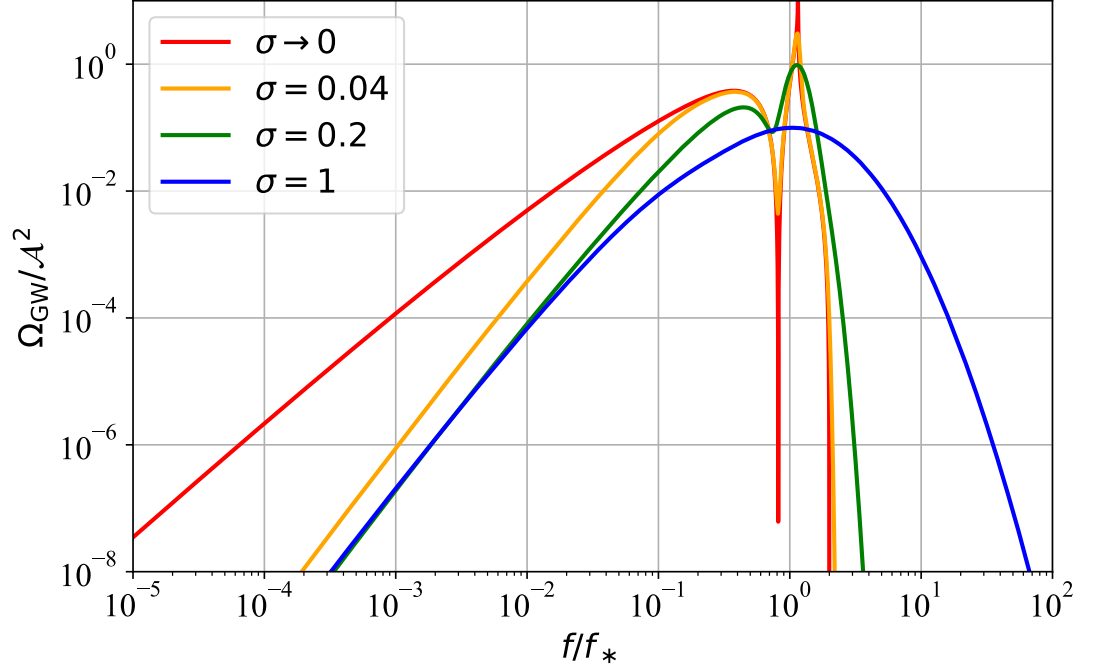


Figure 1. Energy density fraction spectrum of SIGWs normalized with \mathcal{A}^2 . We adopt $\sigma \rightarrow 0$ to label the power spectrum of primordial curvature perturbations in Equation (3). Different choices of σ in Equation (4) are plotted for comparison.

Throughout this paper, we use the measured value of cosmological parameters in the data release 2018 of *Planck* satellite [10]. The publicly available Astropy [48–50] software³ is adopted to evaluate all cosmological quantities. Please note that Equation (5) is one of the leading formulas that will be used during Bayesian analysis in the next section.

3. NANOGrav Constraints on Primordial Curvature Perturbations

When a pulsar timing array (PTA) experiment measures the stochastic gravitational wave background, the timing residual cross-power spectral density is given by $S_{ab}(f) = \Gamma_{ab} h_c^2 / (12\pi^2 f^3)$, which can be shown by combining Equations (1) and (2) in Arzoumanian et al. [51]. Here, Γ_{ab} stands for the overlap reduction function (ORF) that describes the correlation between two pulsars a and b as a function of line-of-sight separation angle between them. Following Equation (17) in Maggiore [52], $h_c(f)$ is the characteristic strain defined as $h_c^2 = 3H_0^2 \Omega_{\text{GW},0} / (2\pi^2 f^2)$, where $H_0 = 100h_0 \text{ km s}^{-1} \text{ Mpc}^{-1}$ is the Hubble constant with h_0 being the reduced Hubble constant. Therefore, the timing residual cross-power spectral density becomes [51]

$$S_{ab} = \Gamma_{ab} \frac{H_0^2 f_{\text{yr}}^{-5}}{8\pi^4} \left(\frac{f}{f_{\text{yr}}} \right)^{-5} \Omega_{\text{GW},0}(f), \quad (7)$$

where f_{yr} is a pivot frequency corresponding to a duration time of 1 year, and the formula for $\Omega_{\text{GW},0}(f)$ is shown in Equation (5). For an isotropic background of GWs, e.g., the SIGWs considered in this work, we take ORF to be the Hellings and Downs coefficients [53].

The timing residual data for a single pulsar is decomposed in its individual constituents, i.e., [54]

$$\delta t = M\epsilon + Fa + Uj + n. \quad (8)$$

The term $M\epsilon$ stands for the inaccuracies in the subtraction of timing model, where M denotes the timing model design matrix, and ϵ is a vector describing small offsets for the timing model parameters. The matrix M is computed through `libstempo` [55]⁴, which is a python interface for TEMP02 [56,57]⁵ timing package. We use the latest Jet Propulsion Laboratory (JPL) solar system ephemeris (SSE) model, DE438 [58], in the timing model fits. The term Fa accounts for all low-frequency signals, including the pulsar-intrinsic red noise. The Fourier design matrix F has alternating sine and cosine functions, and a is a vector comprised of Fourier coefficients at the integer $(1, 2, \dots, N_{\text{mode}})$ multiples of the harmonic base frequency $1/T_s$, where T_s denotes the span between the minimum and maximum time of arrivals (TOAs) in the array [59]. Described by a per-epoch variance (ECORR) for each receiver and backend system [54], the term Uj denotes the white noise which is fully correlated for simultaneous observations at different frequencies, but fully uncorrelated in time. The matrix U maps all TOAs observed simultaneously at different frequencies to a total TOA, and j is the per-epoch white noise which is fully correlated across all observing frequencies. The term n is the timing residual introduced by Gaussian white noise, which is described by the parameters of the TOA uncertainties (EFAC) and an additive variance (EQUAD) for each receiver and backend system [54].

To estimate the allowed parameter space, we perform Bayesian parameter inferences by analyzing a dataset of 45 pulsars in the 12.5-year data release of NANOGrav Collaboration [35]⁶. We list all independent parameters as well as their priors in Table 1. We adopt $N_{\text{mode}} = 30$ frequency bands to the power-law spectrum of pulsar-intrinsic red noise and the common-spectrum process. In practice, we will use the publicly available `enterprise` [60]⁷ to compute the likelihoods and `PTMCMCSampler` [61]⁸ to perform Markov-Chain Monte-Carlo sampling.

Table 1. Priors used in all analyses performed in this paper.

Parameter	Description	Prior	Comment
White Noise			
E_k	EFAC per backend/receiver system	Uniform [0, 10]	single-pulsar analysis only
Q_k [s]	EQUAD per backend/receiver system	log-Uniform [-8.5, -5]	single-pulsar analysis only
J_k [s]	ECORR per backend/receiver system	log-Uniform [-8.5, -5]	single-pulsar analysis only
Red Noise			
A_{red}	power-law spectral amplitude	log-Uniform [-20, -11]	one parameter per pulsar
γ_{red}	power-law spectral index	Uniform [0, 7]	one parameter per pulsar
Primordial curvature perturbations			
$\log \mathcal{A}$	spectral amplitude	Uniform [-3, 0]	one parameter for PTA
$\log f_*$ [Hz]	spectral pivot frequency	Uniform [-10, 0]	one parameter for PTA

Our results are shown in Figure 2, which displays the 95% CL contour plots of $\log \mathcal{A}$ and $\log f_*$ for the power spectra of primordial curvature perturbations with $\sigma \rightarrow 0$ (red solid curve) and $\sigma = 1$ (blue solid curve), respectively. We find that \mathcal{A} has lower limits around 10^{-2} for the two different choices of σ . In contrast, the NANOGrav dataset prefers different frequency bands. For a given value of \mathcal{A} , the frequency range in the case of $\sigma \rightarrow 0$ is almost always larger than that in the case of $\sigma = 1$ by a few times. This result is consistent with the expectations of Figure 1. However, we find strong positive correlations between $\log \mathcal{A}$ and $\log f_*$ in either choice of σ . Furthermore, in Figure 2, we also label the spectral amplitudes that produce the

PBHs with total abundance $\bar{f}_{\text{pbh}} = 1$ (dashed curves) and $\bar{f}_{\text{pbh}} = 10^{-10}$ (dotted curves) that will be interpreted in the next section.

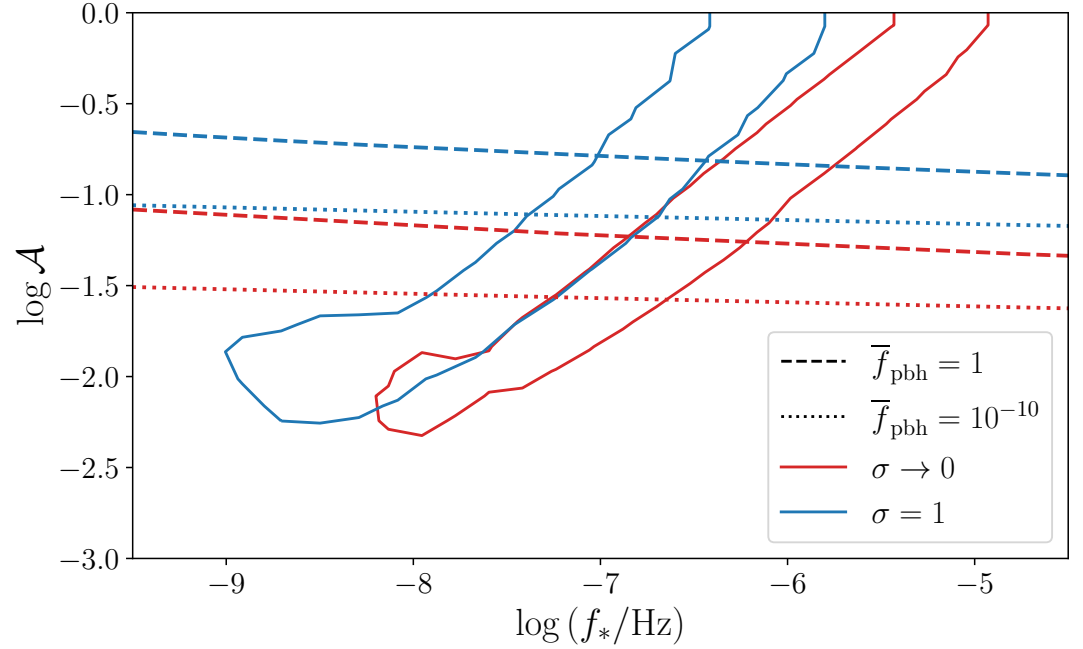


Figure 2. The 95% CL contour plot of \mathcal{A} and f_* inferred from the NANOGrav 12.5yr dataset. Solid curves stand for $\sigma \rightarrow 0$ and $\sigma = 1$, while other curves denote $\bar{f}_{\text{pbh}} = 1$ and $\bar{f}_{\text{pbh}} = 10^{-10}$.

4. Implications for Primordial Black Holes

We define the mass function of PBHs as $f_{\text{pbh}}(m) = \Omega_{\text{dm}}^{-1} d\Omega_{\text{pbh}}/d \ln m$, in which Ω_{dm} and Ω_{pbh} stand for the present energy density fractions of dark matter and PBHs with mass m , respectively. We adopt the concept of critical collapse [62,63] and Press-Schechter formalism [64]. Therefore, following Equation (9) in Wang et al. [43], we have

$$f_{\text{pbh}}(m) = \frac{\Omega_{\text{m}}}{\Omega_{\text{dm}}} \int g(T) \tilde{\beta}(m, m_H) d \ln m_H, \quad (9)$$

where Ω_{m} is the present energy density fraction of non-relativistic matter. Here, we denote

$$g(T) = \frac{g_{*,\rho}(T)}{g_{*,\rho}(T_{\text{eq}})} \frac{g_{*,s}(T_{\text{eq}})}{g_{*,s}(T)} \frac{T}{T_{\text{eq}}}, \quad (10)$$

$$\tilde{\beta}(m, m_H) = \frac{\kappa \mu^{\gamma+1}}{\sqrt{2\pi\gamma}\Delta(k)} \exp\left[-\frac{(\delta_c + \mu)^2}{2\Delta^2(k)}\right], \quad (11)$$

where we have $\mu = [m/(\kappa m_H)]^{1/\gamma}$ with numerical constants $\kappa = 3.3$ and $\gamma = 0.36$, and the critical overdensity for gravitational collapse is $\delta_c = 0.45$. Here, we disregard corrections to δ_c from, e.g., QCD equation of state [65]. The quantity $\tilde{\beta}(m, m_H)$ is a mass distribution function of PBHs, which were produced when the horizon mass was m_H . The subscript eq stands for

cosmological quantities at the epoch of matter-radiation equality. Cosmic temperature T is related to m_H enclosed by the Hubble horizon, i.e., [43]

$$\frac{m_H}{M_\odot} = 4.76 \times 10^{-2} \left(\frac{T}{\text{GeV}} \right)^{-2} \left[\frac{g_{*p}(T)}{106.75} \right]^{-\frac{1}{2}}, \quad (12)$$

where M_\odot denotes the solar mass. We can relate f with m_H by combining Equation (6) with Equation (12) and by reducing T from both equations. The coarse-grained fluctuations in the radiation-dominated cosmos are given by [66,67]

$$\Delta^2(k) = \frac{16}{81} \int d \ln q \left[w\left(\frac{q}{k}\right) \right]^2 \left(\frac{q}{k}\right)^4 \mathcal{T}^2\left(q, \frac{1}{k}\right) \mathcal{P}_{\mathcal{R}}(q), \quad (13)$$

where $w(y) = \exp(-y^2/2)$ is a Gaussian window function and $\mathcal{T}(q, \tau) = 3(\sin x - x \cos x)/x^3$ with $x = q\tau/\sqrt{3}$ is a scalar transfer function. We further define the total abundance of PBHs in dark matter to be $\bar{f}_{\text{pbh}} = \int f_{\text{pbh}}(m) d \ln m$, and define the average mass of PBHs to be $\bar{m} = \int f_{\text{pbh}}(m) dm / \bar{f}_{\text{pbh}}$. The latter roughly displays $\bar{m} \simeq m_*$, where m_* is corresponded to k_* .

Once the constraints on the power spectrum of primordial curvature perturbations are obtained, as shown in Figure 2, we can recast them into constraints on the mass function of PBHs, or more precisely, on the average mass and total abundance of PBHs. We show the results in Figure 3. The shaded regions are allowed by the NANOGrav 12.5-year dataset for $\sigma \rightarrow 0$ (red region) and $\sigma = 1$ (blue region). When at least one fraction (e.g., $f_{\text{pbh}} = 10^{-10}$) of dark matter is composed of PBHs, the mass range $2 \times 10^{-4} - 10^{-2} M_\odot$ ($4 \times 10^{-3} - 0.2 M_\odot$) for $\sigma \rightarrow 0$ ($\sigma = 1$) is preferred by the current dataset. Based on Figure 3 in Wang et al. [43], we find that these mass ranges can be cross-checked with high-precision by observing the GWs emitted from inspiraling stage of PBH binaries. In addition, they might be further tested by measuring the anisotropies in stochastic gravitational-wave background (SGWB) [68]. For comparison, we also depict the existing upper limit (cyan curve) on the mass function of PBHs, as reviewed in Carr et al. [15]. We find the SIGW probe to be more powerful than electromagnetic probes, implying that a larger parameter space can be explored with the SIGW probe. This can also be understood by revisiting Figure 2, in which we depicted the curves labeling $\bar{f}_{\text{pbh}} = 10^{-10}$. The latter is corresponded to $\mathcal{A} \simeq \text{few} \times 10^{-2}$. In contrast, the NANOGrav experiment has reached $\mathcal{A} \simeq 10^{-2}$ in the most sensitive frequency band $\sim (10^{-9} - 10^{-8})$ Hz.

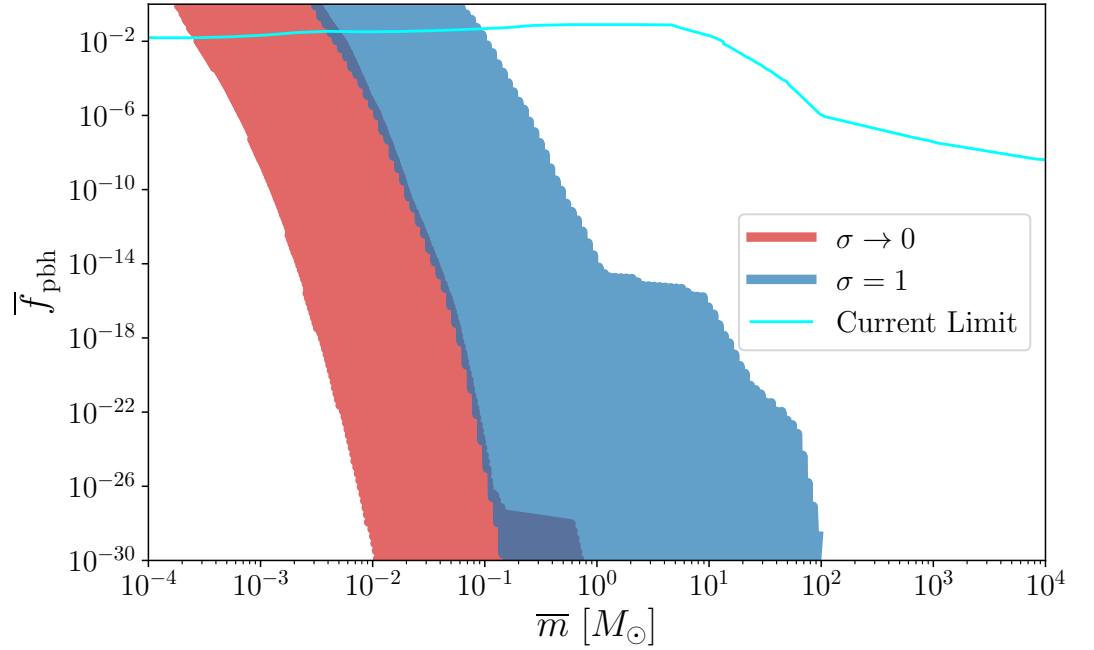


Figure 3. The NANOGrav constraints on the averaged mass and total abundance of PBHs. Shaded regions are allowed by the NANOGrav dataset for $\sigma \rightarrow 0$ and $\sigma = 1$. Cyan curve denotes the existing upper limit on the mass function of PBHs [15].

5. Constraints from Ongoing and Planned Gravitational-Wave Detectors

In the future, the power spectrum of primordial curvature perturbations and the mass function of PBHs, which remain unknown until now, can be further explored with ongoing and planned GW experiments, such as Square Kilometer Array (SKA) [69–71], μ Ares [72], Laser Interferometer Space Antenna (LISA) [73,74], Big Bang Observer (BBO) [75,76], Deci-hertz Interferometer Gravitational wave Observatory (DECIGO) [77,78], Einstein Telescope (ET) [79] and Advanced LIGO and Virgo [26–28]. Such multi-band observations could explore all possible parameter spaces of primordial curvature perturbations and PBHs. Other experiments are not considered in this work, but our method can be generalized straightforwardly to study them, if needed.

To estimate the sensitivity curve of a given GW experiment consisting of n_{det} detectors, we define an optimal signal-to-noise ratio (SNR) denoted with ρ as follows [80]

$$\rho^2 = n_{\text{det}} T_{\text{obs}} \int_{f_{\text{min}}}^{f_{\text{max}}} \left[\frac{S_{\text{GW}}(f)}{S_n^{\text{eff}}(f)} \right]^2 df, \quad (14)$$

where T_{obs} is a duration time of observing run, the power spectral density (PSD) of SIGWs is defined as

$$S_{\text{GW}}(f) = \left(\frac{3H_0^2}{2\pi^2 f^3} \right) \Omega_{\text{GW},0}(f), \quad (15)$$

and the effective noise PSD of the detector network is denoted as $S_n^{\text{eff}}(f)$ that is a function of f . The concrete setups of aforementioned experiments are summarized in Table 2 of Ref. [81] and references therein. We consider a single detector for LISA, two independent detectors for μ Ares, BBO and DECIGO, three detectors for ET, and 200 pulsars for SKA. For comparison, we

consider one detector for Advanced LIGO with an observing duration of four years and 100% duty circle.

Given a desired value of SNR, which is unity in this work, we obtain the minimal detectable \mathcal{A}_{\min} for the given experiment by resolving Equation (14). Since $\Omega_{\text{GW},0}(f)$ is uniquely determined by \mathcal{A} and f_* , we depict the theoretical expectation of \mathcal{A}_{\min} in the $\mathcal{A} - f_*$ plane in Figures 4 and 5 for the choices of $\sigma \rightarrow 0$ and $\sigma = 1$, respectively. For comparison, we plot the exclusion region on \mathcal{A} from the Advanced LIGO and Virgo first three observing runs (red shaded) [82].

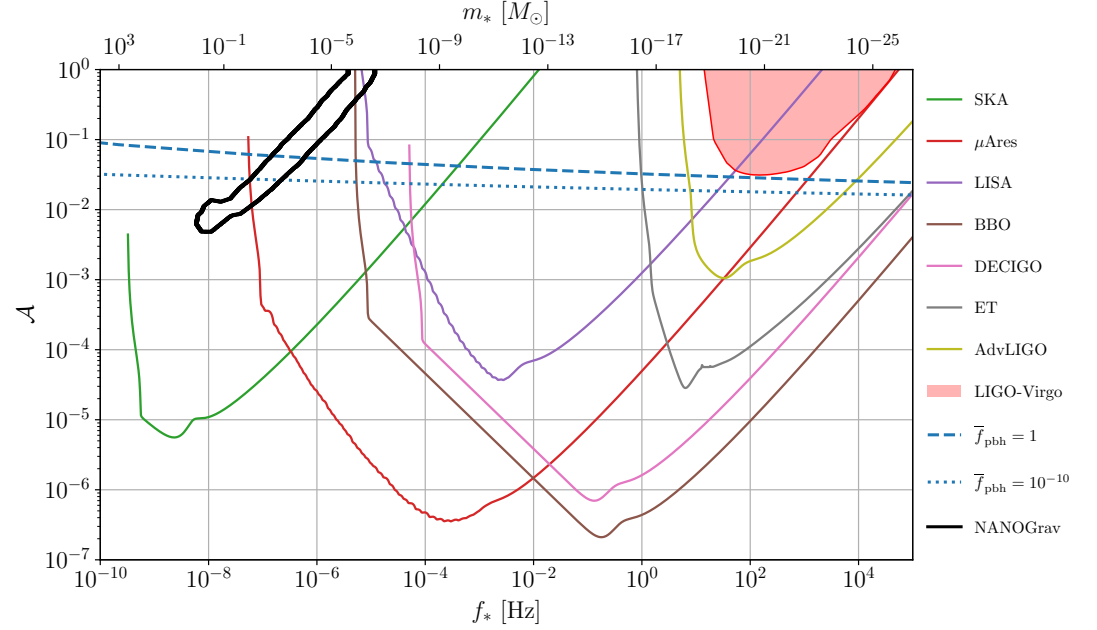


Figure 4. Sensitivities of ongoing and planned GW experiments on measurements of the power spectrum of primordial curvature perturbations with $\sigma \rightarrow 0$. The excluded region by Advanced LIGO–Virgo first three observing runs [82] is shown for comparison. We show the allowed region from NANOGrav 12.5-year dataset, as shown in Figure 2. We also depict critical curves corresponded to $\bar{f}_{\text{pbh}} = 1$ and $\bar{f}_{\text{pbh}} = 10^{-10}$.

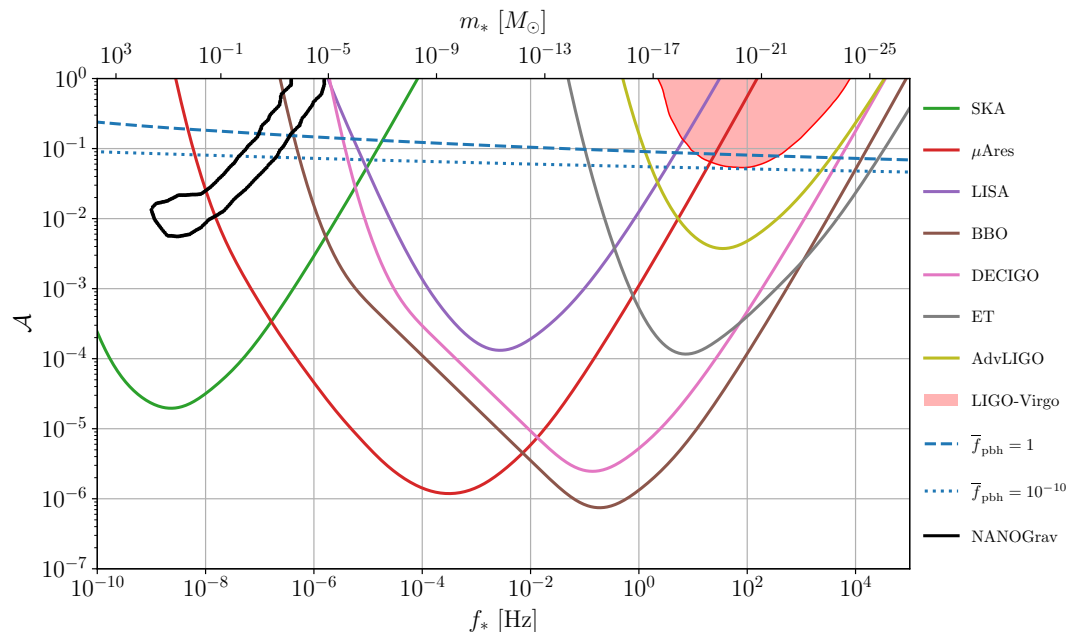


Figure 5. The same as Figure 4 but $\sigma = 1$.

Based on Figures 4 and 5, we find that the regions allowed by the current dataset of NANOGrav (enclosed by black curves) can be thoroughly tested with SKA and μ Ares. Smaller values of \mathcal{A} , i.e., $\sim(10^{-4} - 10^{-7})$, are also expected to be reached by the planned GW experiments. The sensitivity of Advanced LIGO to measure the SIGWs is expected to be improved by one order of magnitude in upcoming observing runs. If other values of SNR are desired, we can obtain revised \mathcal{A}_{\min} by rescaling the above results by multiplying a factor of $(\text{SNR})^{1/2}$. After recasting the expected constraints on \mathcal{A} into constraints on the mass function of PBHs, we further find that the full parameter space of PBHs, that account for at least a fraction of dark matter, e.g., $f_{\text{pbh}} \sim 10^{-10}$, can be thoroughly explored with multi-band GW measurements, e.g., a detector network composed of SKA, μ Ares and ET, or other detector networks. Therefore, we expect that the scenario of PBHs as a candidate of dark matter can be supported or vetoed by future GW observations.

6. Conclusions and Discussion

In this work, we obtained new constraints on the power spectrum of primordial curvature perturbations and the mass function of PBHs by searching for the energy density fraction spectrum of SIGWs in the NANOGrav 12.5-year dataset. We found the lower limits on \mathcal{A} , namely, $\mathcal{A} \gtrsim 10^{-2}$ and showed the 95% CL contours of \mathcal{A} and f_* (see Figure 2). Recasting these contours into the PBH mass-abundance plane, we showed the parameter space of PBHs allowed by the NANOGrav (see Figure 3). We found that at least a fraction of dark matter can be interpreted with the scenario of PBHs in the mass range $\sim(10^{-4} - 10^{-1})M_{\odot}$. We also studied dependence of the above results on the value of σ . Furthermore, this mass range is expected to be cross-checked with high-precision by observing the GWs from PBH mergers (see Figure 3 in Wang et al. [43]). We also found that the SIGW probe is much more powerful than other probes to search for the PBHs.

We further forecasted the sensitivity curves of ongoing and planned GW experiments on detection of PBHs and the primordial curvature perturbations by searching for SIGWs. We found that the primordial curvature perturbations with spectral amplitude larger than $\sim(10^{-4} - 10^{-7})$ can be measured with planned GW detection programs. The sensitivity of

Advanced LIGO-Virgo to detect the SIGWs was expected to be improved by one order of magnitude in the near future. This prediction may promote extensive investigations of cosmic inflation at late-time stages. Meanwhile, the scenario of PBHs within almost whole mass range can be thoroughly tested, since the critical spectral amplitude to form the PBHs is much larger than 10^{-4} (see Figures 4 and 5). In particular, we can search for the PBHs within mass range $(10^{-16} - 10^{-11})M_{\odot}$, which can compose all of the dark matter and otherwise are beyond capabilities of other probes. In addition, we emphasized the importance of multi-band GW detector networks for accomplishing the above theoretical expectations.

In this paper, we made several assumptions to simplify our computations. First, we disregarded possible contributions of primordial non-Gaussianity to the formation of PBHs [46, 83–86] and to the production of SIGWs [45]. It is an interesting topic to study the primordial non-Gaussianity, deserving an independent work. Second, we took into account the median value of the effective relativistic degrees of freedom of the early Universe, but disregarded their uncertainties [47]. In fact, changing the above two assumptions could alter the mass function of PBHs and the energy density fraction spectrum of SIGWs. We would leave a possible study of this question to future works. Third, we disregarded contributions of nonlinear cosmological perturbations to the energy density fraction spectrum of SIGWs, since there is not a complete theory of SIGWs at the third order [87–91]. We might revisit this assumption in future, once the theory is complete.

Author Contributions: Conceptualization, S.W.; methodology, Z.C.Z. and S.W.; software, Z.C.Z.; validation, Z.C.Z. and S.W.; formal analysis, Z.C.Z. and S.W.; investigation, Z.C.Z. and S.W.; resources, S.W.; data curation, Z.C.Z.; writing—original draft preparation, S.W.; writing—review and editing, Z.C.Z. and S.W.; visualization, Z.C.Z. and S.W.; supervision, S.W.; project administration, S.W.; funding acquisition, Z.C.Z. and S.W.. All authors have read and agreed to the published version of the manuscript.

Funding: This research was funded by the National Natural Science Foundation of China grant number 12175243 and grant number 12005016, the Key Research Program of the Chinese Academy of Sciences grant number XDPB15, and the science research grants from the China Manned Space Project grant number CMS-CSST-2021-B01.

Data Availability Statement: Publicly available datasets were analyzed in this study. This data can be found here: <https://data.nanograv.org>

Acknowledgments: We acknowledge Zu-Cheng Chen, Jun-Peng Li and Ke Wang for helpful discussions.

Conflicts of Interest: The authors declare no conflict of interest.

Notes

- 1 <http://data.nanograv.org>, version v3
- 2 <https://member.ipmu.jp/satoshi.shirai/EOS2018.php>, accessed on 1 January 2019
- 3 <https://www.astropy.org/>, version 5.1
- 4 <https://vallis.github.io/libstempo/>, version 2.4.5
- 5 <https://bitbucket.org/psrsoft/tempo2.git>, version 2021.07.1
- 6 https://github.com/nanograv/12p5yr_stochastic_analysis, accessed on 1 January 2022
- 7 <https://zenodo.org/record/4059815>, version 3.2.3
- 8 <https://zenodo.org/record/1037579>, version 2.0.0

References

1. Hawking, S. Gravitationally collapsed objects of very low mass. *Mon. Not. Roy. Astron. Soc.* **1971**, *152*, 75.
2. Khlopov, M.Y. Primordial Black Holes. *Res. Astron. Astrophys.* **2010**, *10*, 495–528. <https://doi.org/10.1088/1674-4527/10/6/001>.
3. Belotsky, K.M.; Dmitriev, A.D.; Esipova, E.A.; Gani, V.A.; Grobov, A.V.; Khlopov, M.Y.; Kirillov, A.A.; Rubin, S.G.; Svadkovsky, I.V. Signatures of primordial black hole dark matter. *Mod. Phys. Lett. A* **2014**, *29*, 1440005. <https://doi.org/10.1142/S0217732314400057>.

4. Franciolini, G.; Musco, I.; Pani, P.; Urbano, A. From inflation to black hole mergers and back again: Gravitational-wave data-driven constraints on inflationary scenarios with a first-principle model of primordial black holes across the QCD epoch. *arXiv* **2022**, arXiv:2209.05959.
5. Musco, I.; De Luca, V.; Franciolini, G.; Riotto, A. Threshold for primordial black holes. II. A simple analytic prescription. *Phys. Rev. D* **2021**, *103*, 063538. <https://doi.org/10.1103/PhysRevD.103.063538>.
6. Guth, A.H. The Inflationary Universe: A Possible Solution to the Horizon and Flatness Problems. *Phys. Rev.* **1981**, *D23*, 347–356. <https://doi.org/10.1103/PhysRevD.23.347>.
7. Linde, A.D. A New Inflationary Universe Scenario: A Possible Solution of the Horizon, Flatness, Homogeneity, Isotropy and Primordial Monopole Problems. *Phys. Lett.* **1982**, *108B*, 389–393. [https://doi.org/10.1016/0370-2693\(82\)91219-9](https://doi.org/10.1016/0370-2693(82)91219-9).
8. Starobinsky, A.A. A New Type of Isotropic Cosmological Models Without Singularity. *Phys. Lett.* **1980**, *B91*, 99–102. [https://doi.org/10.1016/0370-2693\(80\)90670-X](https://doi.org/10.1016/0370-2693(80)90670-X).
9. Hinshaw, G.; Larson, D.; Komatsu, E.; Spergel, D.N.; Bennett, C.L.; Dunkley, J.; Nolta, M.R.; Halpern, M.; Hill, R.S.; Odegard, N. Nine-Year Wilkinson Microwave Anisotropy Probe (WMAP) Observations: Cosmological Parameter Results. *Astrophys. J. Suppl.* **2013**, *208*, 19. <https://doi.org/10.1088/0067-0049/208/2/19>.
10. Aghanim, N.; Larson, D.; Komatsu, E.; Sperge, D.N.; Bennett, C.L.; Dunkley, J.; Nolta, M.R.; Halpern, M.; Hill, R.S.; Odegard, N. Planck 2018 results. VI. Cosmological parameters. *Astron. Astrophys.* **2020**, *641*, A6; Erratum in *Astron. Astrophys.* **2021**, *652*, C4. <https://doi.org/10.1051/0004-6361/201833910>.
11. Alam, S.; Ata, M.; Bailey, S.; Beutler, F.; Bizyaev, D.; Blazek, J.A.; Bolton, A.S.; Brownstein, J.R.; Burden, A.; Chuang, C.-H. The clustering of galaxies in the completed SDSS-III Baryon Oscillation Spectroscopic Survey: Cosmological analysis of the DR12 galaxy sample. *Mon. Not. Roy. Astron. Soc.* **2017**, *470*, 2617–2652, <https://doi.org/10.1093/mnras/stx721>.
12. Abbott, T.M.C. et al. [DES Collaboration] Dark Energy Survey Year 3 results: Cosmological constraints from galaxy clustering and weak lensing. *Phys. Rev. D* **2022**, *105*, 023520, <https://doi.org/10.1103/PhysRevD.105.023520>.
13. Carr, B.J.; Hawking, S.W. Black holes in the early Universe. *Mon. Not. Roy. Astron. Soc.* **1974**, *168*, 399–415. <https://doi.org/10.1093/mnras/168.2.399>.
14. Chapline, G.F. Cosmological effects of primordial black holes. *Nature* **1975**, *253*, 251–252. <https://doi.org/10.1038/253251a0>.
15. Carr, B.; Kohri, K.; Sendouda, Y.; Yokoyama, J. Constraints on primordial black holes. *Rept. Prog. Phys.* **2021**, *84*, 116902, <https://doi.org/10.1088/1361-6633/ac1e31>.
16. Escrivà, A.; Kuhnel, F.; Tada, Y. Primordial Black Holes. *arXiv* **2022**, arXiv:2211.05767.
17. Kohri, K.; Sekiguchi, T.; Wang, S. Cosmological 21-cm line observations to test scenarios of super-Eddington accretion on to black holes being seeds of high-redshifted supermassive black holes. *Phys. Rev. D* **2022**, *106*, 043539. <https://doi.org/10.1103/PhysRevD.106.043539>.
18. Sasaki, M.; Suyama, T.; Tanaka, T.; Yokoyama, S. Primordial Black Hole Scenario for the Gravitational-Wave Event GW150914. *Phys. Rev. Lett.* **2016**, *117*, 061101. <https://doi.org/10.1103/PhysRevLett.117.061101>.
19. Raidal, M.; Vaskonen, V.; Veermäe, H. Gravitational Waves from Primordial Black Hole Mergers. *JCAP* **2017**, *09*, 037. <https://doi.org/10.1088/1475-7516/2017/09/037>.
20. Ali-Haïmoud, Y.; Kovetz, E.D.; Kamionkowski, M. Merger rate of primordial black-hole binaries. *Phys. Rev. D* **2017**, *96*, 123523. <https://doi.org/10.1103/PhysRevD.96.123523>.
21. Chen, Z.C.; Huang, Q.G. Merger Rate Distribution of Primordial-Black-Hole Binaries. *Astrophys. J.* **2018**, *864*, 61. <https://doi.org/10.3847/1538-4357/aad6e2>.
22. Nishikawa, H.; Kovetz, E.D.; Kamionkowski, M.; Silk, J. Primordial-black-hole mergers in dark-matter spikes. *Phys. Rev.* **2019**, *D99*, 043533. <https://doi.org/10.1103/PhysRevD.99.043533>.
23. Bird, S.; Cholis, I.; Muñoz, J.B.; Ali-Haimoud, Y.; Kamionkowski, M.; Kovetz, E.D.; Raccanelli, A.; Riess, A.G. Did LIGO detect dark matter? *Phys. Rev. Lett.* **2016**, *116*, 201301. <https://doi.org/10.1103/PhysRevLett.116.201301>.
24. Wang, S.; Zhao, Z.C. GW200105 and GW200115 are compatible with a scenario of primordial black hole binary coalescences. *Eur. Phys. J. C* **2022**, *82*, 9. <https://doi.org/10.1140/epjc/s10052-021-09981-1>.
25. Belotsky, K.M.; Dokuchaev, V.I.; Eroshenko, Y.N.; Esipova, E.A.; Khlopov, M.Y.; Khromykh, L.A.; Kirillov, A.A.; Nikulin, V.V.; Rubin, S.G.; Svadkovsky, I.V. Clusters of primordial black holes. *Eur. Phys. J. C* **2019**, *79*, 246. <https://doi.org/10.1140/epjc/s10052-019-6741-4>.
26. Harry, G.M. Advanced LIGO: The next generation of gravitational wave detectors. *Class. Quant. Grav.* **2010**, *27*, 084006. <https://doi.org/10.1088/0264-9381/27/8/084006>.
27. Acernese, F.; Agathos, M.; Agatsuma, K.; Aisa, D.; Allemandou, N.; Allocca, A.; Amarni, J.; Astone, P.; Balestri, G.; Ballardin, G. Advanced Virgo: A second-generation interferometric gravitational wave detector. *Class. Quant. Grav.* **2015**, *32*, 024001. <https://doi.org/10.1088/0264-9381/32/2/024001>.
28. Somiya, K. Detector configuration of KAGRA: The Japanese cryogenic gravitational-wave detector. *Class. Quant. Grav.* **2012**, *29*, 124007. <https://doi.org/10.1088/0264-9381/29/12/124007>.

29. Mollerach, S.; Harari, D.; Matarrese, S. CMB polarization from secondary vector and tensor modes. *Phys. Rev.* **2004**, *D69*, 063002. <https://doi.org/10.1103/PhysRevD.69.063002>.
30. Ananda, K.N.; Clarkson, C.; Wands, D. The Cosmological gravitational wave background from primordial density perturbations. *Phys. Rev.* **2007**, *D75*, 123518. <https://doi.org/10.1103/PhysRevD.75.123518>.
31. Baumann, D.; Steinhardt, P.J.; Takahashi, K.; Ichiki, K. Gravitational Wave Spectrum Induced by Primordial Scalar Perturbations. *Phys. Rev.* **2007**, *D76*, 084019. <https://doi.org/10.1103/PhysRevD.76.084019>.
32. Assadullahi, H.; Wands, D. Constraints on primordial density perturbations from induced gravitational waves. *Phys. Rev.* **2010**, *D81*, 023527. <https://doi.org/10.1103/PhysRevD.81.023527>.
33. Kohri, K.; Terada, T. Semianalytic calculation of gravitational wave spectrum nonlinearly induced from primordial curvature perturbations. *Phys. Rev.* **2018**, *D97*, 123532. <https://doi.org/10.1103/PhysRevD.97.123532>.
34. Espinosa, J.R.; Racco, D.; Riotto, A. A Cosmological Signature of the SM Higgs Instability: Gravitational Waves. *JCAP* **2018**, *09*, 012. <https://doi.org/10.1088/1475-7516/2018/09/012>.
35. Arzoumanian, Z.; Baker, P.T.; Blumer, H.; Bécsy, B.; Brazier, A.; Brook, P.R.; Burke-Spolaor, S.; Chatterjee, S.; Chen, S.; Cordes, J.M. The NANOGrav 12.5 yr Data Set: Search for an Isotropic Stochastic Gravitational-wave Background. *Astrophys. J. Lett.* **2020**, *905*, L34. <https://doi.org/10.3847/2041-8213/abd401>.
36. De Luca, V.; Franciolini, G.; Riotto, A. NANOGrav Data Hints at Primordial Black Holes as Dark Matter. *Phys. Rev. Lett.* **2021**, *126*, 041303. <https://doi.org/10.1103/PhysRevLett.126.041303>.
37. Vaskonen, V.; Veermäe, H. Did NANOGrav see a signal from primordial black hole formation? *Phys. Rev. Lett.* **2021**, *126*, 051303. <https://doi.org/10.1103/PhysRevLett.126.051303>.
38. Kohri, K.; Terada, T. Solar-Mass Primordial Black Holes Explain NANOGrav Hint of Gravitational Waves. *Phys. Lett. B* **2021**, *813*, 136040. <https://doi.org/10.1016/j.physletb.2020.136040>.
39. Domènech, G.; Pi, S. NANOGrav hints on planet-mass primordial black holes. *Sci. China Phys. Mech. Astron.* **2022**, *65*, 230411. <https://doi.org/10.1007/s11433-021-1839-6>.
40. Atal, V.; Sanglas, A.; Triantafyllou, N. NANOGrav signal as mergers of Stupendously Large Primordial Black Holes. *JCAP* **2021**, *06*, 022. <https://doi.org/10.1088/1475-7516/2021/06/022>.
41. Yi, Z.; Fei, Q. Constraints on primordial curvature spectrum from primordial black holes and scalar-induced gravitational waves. *arXiv* **2022**, arXiv:2210.03641.
42. Maggiore, M. *Gravitational Waves. Volume 1: Theory and Experiments*; Oxford Master Series in Physics; Oxford University Press: Oxford, UK, 2007.
43. Wang, S.; Terada, T.; Kohri, K. Prospective constraints on the primordial black hole abundance from the stochastic gravitational-wave backgrounds produced by coalescing events and curvature perturbations. *Phys. Rev. D* **2019**, *99*, 103531. <https://doi.org/10.1103/PhysRevD.99.103531>.
44. Bugaev, E.; Klimai, P. Induced gravitational wave background and primordial black holes. *Phys. Rev. D* **2010**, *81*, 023517. <https://doi.org/10.1103/PhysRevD.81.023517>.
45. Adshead, P.; Lozanov, K.D.; Weiner, Z.J. Non-Gaussianity and the induced gravitational wave background. *JCAP* **2021**, *10*, 080. <https://doi.org/10.1088/1475-7516/2021/10/080>.
46. Ferrante, G.; Franciolini, G.; Iovino, Junior, A.; Urbano, A. Primordial non-gaussianity up to all orders: Theoretical aspects and implications for primordial black hole models. *arXiv* **2022**, arXiv:2211.01728.
47. Saikawa, K.; Shirai, S. Primordial gravitational waves, precisely: The role of thermodynamics in the Standard Model. *JCAP* **2018**, *1805*, 035. <https://doi.org/10.1088/1475-7516/2018/05/035>.
48. Robitaille, T.P. et al. [The Astropy Collaboration] Astropy: A Community Python Package for Astronomy. *Astron. Astrophys.* **2013**, *558*, A33. <https://doi.org/10.1051/0004-6361/201322068>.
49. Price-Whelan, A.M. et al. [The Astropy Collaboration] The Astropy Project: Building an Open-science Project and Status of the v2.0 Core Package. *Astron. J.* **2018**, *156*, 123. <https://doi.org/10.3847/1538-3881/aabc4f>.
50. Price-Whelan, A.M. et al. [The Astropy Collaboration] The Astropy Project: Sustaining and Growing a Community-oriented Open-source Project and the Latest Major Release (v5.0) of the Core Package*. *Astrophys. J.* **2022**, *935*, 167. <https://doi.org/10.3847/1538-4357/ac7c74>.
51. Arzoumanian, Z.; Baker, P.T.; Brazier, A.; Burke-Spolaor, S.; Chamberlin, S.J.; Chatterjee, S.; Christy, B.; Cordes, J.M.; Cornish, N.J.; Crawford, F.; et al. The NANOGrav 11-year Data Set: Pulsar-timing Constraints on the Stochastic Gravitational-wave Background. *Astrophys. J.* **2018**, *859*, 47. <https://doi.org/10.3847/1538-4357/aabd3b>.
52. Maggiore, M. Gravitational wave experiments and early universe cosmology. *Phys. Rept.* **2000**, *331*, 283–367. [https://doi.org/10.1016/S0370-1573\(99\)00102-7](https://doi.org/10.1016/S0370-1573(99)00102-7).
53. Hellings, R.W.; Downs, G.S. Upper limits on the isotropic gravitational radiation background from pulsar timing analysis. *Astrophys. J. Lett.* **1983**, *265*, L39–L42. <https://doi.org/10.1086/183954>.

54. Arzoumanian, Z.; Brazier, A.; Burke-Spolaor, S.; Chamberlin, S.; Chatterjee, S.; Christy, B.; Cordes, J.; Cornish, N.; Demorest, P.; Deng, X.; et al. The NANOGrav Nine-year Data Set: Limits on the Isotropic Stochastic Gravitational Wave Background. *Astrophys. J.* **2016**, *821*, 13. <https://doi.org/10.3847/0004-637X/821/1/13>.
55. Michele, V. Libstempo: Python Wrapper for Tempo2. Astrophysics Source Code Library, Record ascl:2002.017. 2020. <https://bitbucket.org/psrsoft/tempo2.git>.
56. Hobbs, G.; Edwards, R.T.; Manchester, R.N. Tempo2, a new pulsar timing package. 1. overview. *Mon. Not. Roy. Astron. Soc.* **2006**, *369*, 655–672. <https://doi.org/10.1111/j.1365-2966.2006.10302.x>.
57. Edwards, R.T.; Hobbs, G.B.; Manchester, R.N. Tempo2, a new pulsar timing package. 2. The timing model and precision estimates. *Mon. Not. Roy. Astron. Soc.* **2006**, *372*, 1549–1574. <https://doi.org/10.1111/j.1365-2966.2006.10870.x>.
58. Folkner, W.M.; Park, R.S. *Planetary Ephemeris DE438 for Juno*; Technical Report IOM 392R-18-004; CAJet Propulsion Laboratory: Pasadena, CA, USA, 2018.
59. van Haasteren, R.; Vallisneri, M. New advances in the Gaussian-process approach to pulsar-timing data analysis. *Phys. Rev. D* **2014**, *90*, 104012. <https://doi.org/10.1103/PhysRevD.90.104012>.
60. Ellis, J.A.; Vallisneri, M.; Taylor, S.R.; Baker, P.T. *ENTERPRISE: Enhanced Numerical Toolbox Enabling a Robust Pulsar Inference Suite*; Zenodo: Genève, Switzerland, 2020. <https://doi.org/10.5281/zenodo.4059815>.
61. Ellis, J.; van Haasteren, R. *jellis18/PTMCMCSampler: Official Release*; Zenodo: Genève, Switzerland, 2017. <https://doi.org/10.5281/zenodo.1037579>.
62. Carr, B.; Kuhnel, F.; Sandstad, M. Primordial Black Holes as Dark Matter. *Phys. Rev.* **2016**, *D94*, 083504. <https://doi.org/10.1103/PhysRevD.94.083504>.
63. Yokoyama, J. Cosmological constraints on primordial black holes produced in the near critical gravitational collapse. *Phys. Rev.* **1998**, *D58*, 107502. <https://doi.org/10.1103/PhysRevD.58.107502>.
64. Press, W.H.; Schechter, P. Formation of galaxies and clusters of galaxies by selfsimilar gravitational condensation. *Astrophys. J.* **1974**, *187*, 425–438. <https://doi.org/10.1086/152650>.
65. Byrnes, C.T.; Hindmarsh, M.; Young, S.; Hawkins, M.R.S. Primordial black holes with an accurate QCD equation of state. *JCAP* **2018**, *08*, 041. <https://doi.org/10.1088/1475-7516/2018/08/041>.
66. Young, S.; Byrnes, C.T.; Sasaki, M. Calculating the mass fraction of primordial black holes. *JCAP* **2014**, *1407*, 045. <https://doi.org/10.1088/1475-7516/2014/07/045>.
67. Ando, K.; Inomata, K.; Kawasaki, M. Primordial black holes and uncertainties in the choice of the window function. *Phys. Rev.* **2018**, *D97*, 103528. <https://doi.org/10.1103/PhysRevD.97.103528>.
68. Wang, S.; Vardanyan, V.; Kohri, K. Probing primordial black holes with anisotropies in stochastic gravitational-wave background. *arXiv* **2021**, arXiv:2107.01935.
69. Dewdney, P.E.; Hall, P.J.; Schilizzi, R.T.; Lazio, T.J.L. The square kilometre array. *Proc. IEEE* **2009**, *97*, 1482–1496.
70. Weltman, A.; Bull, P.; Camera, S.; Kelley, K.; Padmanabhan, H.; Pritchard, J.; Raccanelli, A.; Riemer-Sørensen, S.; Shao, L.; Andrianomena, S.; et al. Fundamental physics with the Square Kilometre Array. *Publ. Astron. Soc. Austral.* **2020**, *37*, e002. <https://doi.org/10.1017/pasa.2019.42>.
71. Moore, C.J.; Cole, R.H.; Berry, C.P.L. Gravitational-wave sensitivity curves. *Class. Quant. Grav.* **2015**, *32*, 015014. <https://doi.org/10.1088/0264-9381/32/1/015014>.
72. Sesana, A.; Korsakova, N.; Sedda, M.A.; Baibhav, V.; Barausse, E.; Barke, S.; Berti, E.; Bonetti, M.; Capelo, P.R.; Caprini, C.; et al. Unveiling the gravitational universe at μ -Hz frequencies. *Exper. Astron.* **2021**, *51*, 1333–1383. <https://doi.org/10.1007/s10686-021-09709-9>.
73. Amaro-Seoane, P.; Audley, H.; Babak, S.; Baker, J.; Barausse, E.; Bender, P.; Berti, E.; Binetruy, P.; Born, M.; Bortoluzzi, D.; et al. Laser Interferometer Space Antenna. *arXiv* **2017**, arXiv:1702.00786.
74. Robson, T.; Cornish, N.J.; Liu, C. The construction and use of LISA sensitivity curves. *Class. Quant. Grav.* **2019**, *36*, 105011. <https://doi.org/10.1088/1361-6382/ab1101>.
75. Crowder, J.; Cornish, N.J. Beyond LISA: Exploring future gravitational wave missions. *Phys. Rev. D* **2005**, *72*, 083005. <https://doi.org/10.1103/PhysRevD.72.083005>.
76. Harry, G.M.; Fritschel, P.; Shaddock, D.A.; Folkner, W.; Phinney, E.S. Laser interferometry for the big bang observer. *Class. Quant. Grav.* **2006**, *23*, 4887–4894. <https://doi.org/10.1088/0264-9381/23/15/008>.
77. Sato, S.; Seiji, K.; Masaki, A.; Takashi, N.; Kimio, T.; Akito, A.; Ikkoh, F.; Kunihito, I.; Nobuyuki, K.; Shigenori, M.; et al. The status of DECIGO. *J. Phys. Conf. Ser.* **2017**, *840*, 012010. <https://doi.org/10.1088/1742-6596/840/1/012010>.
78. Kawamura, S.; Ando, M.; Seto, N.; Sato, S.; Musha, M.; Kawano, I.; Yokoyama, J.; Tanaka, T.; Ioka, K.; Akutsu, T.; et al. Current status of space gravitational wave antenna DECIGO and B-DECIGO. *PTEP* **2021**, *2021*, 05A105. <https://doi.org/10.1093/ptep/ptab019>.
79. Punturo, M.; Abernathy, M.; Acernese, F.; Allen, B.; Andersson, N.; Arun, K.; Barone, F.; Barr, B.; Barsuglia, M.; Beker, M. The Einstein Telescope: A third-generation gravitational wave observatory. *Class. Quant. Grav.* **2010**, *27*, 194002. <https://doi.org/10.1088/0264-9381/27/19/194002>.

80. Schmitz, K. New Sensitivity Curves for Gravitational-Wave Signals from Cosmological Phase Transitions. *JHEP* **2021**, *01*, 097. [https://doi.org/10.1007/JHEP01\(2021\)097](https://doi.org/10.1007/JHEP01(2021)097).
81. Campeti, P.; Komatsu, E.; Poletti, D.; Baccigalupi, C. Measuring the spectrum of primordial gravitational waves with CMB, PTA and Laser Interferometers. *JCAP* **2021**, *01*, 012. <https://doi.org/10.1088/1475-7516/2021/01/012>.
82. Romero-Rodriguez, A.; Martinez, M.; Pujolàs, O.; Sakellariadou, M.; Vaskonen, V. Search for a Scalar Induced Stochastic Gravitational Wave Background in the Third LIGO-Virgo Observing Run. *Phys. Rev. Lett.* **2022**, *128*, 051301. <https://doi.org/10.1103/PhysRevLett.128.051301>.
83. Franciolini, G.; Kehagias, A.; Matarrese, S.; Riotto, A. Primordial Black Holes from Inflation and non-Gaussianity. *JCAP* **2018**, *03*, 016. <https://doi.org/10.1088/1475-7516/2018/03/016>.
84. Gow, A.D.; Assadullahi, H.; Jackson, J.H.P.; Koyama, K.; Vennin, V.; Wands, D. Non-perturbative non-Gaussianity and primordial black holes. *arXiv* **2022**, arXiv:2211.08348.
85. Cai, Y.F.; Ma, X.H.; Sasaki, M.; Wang, D.G.; Zhou, Z. Highly non-Gaussian tails and primordial black holes from single-field inflation. *arXiv* **2022**, arXiv:2207.11910.
86. Kitajima, N.; Tada, Y.; Yokoyama, S.; Yoo, C.M. Primordial black holes in peak theory with a non-Gaussian tail. *JCAP* **2021**, *10*, 053. <https://doi.org/10.1088/1475-7516/2021/10/053>.
87. Yuan, C.; Chen, Z.C.; Huang, Q.G. Probing primordial–black-hole dark matter with scalar induced gravitational waves. *Phys. Rev. D* **2019**, *100*, 081301. <https://doi.org/10.1103/PhysRevD.100.081301>.
88. Zhou, J.Z.; Zhang, X.; Zhu, Q.H.; Chang, Z. The third order scalar induced gravitational waves. *JCAP* **2022**, *05*, 013. <https://doi.org/10.1088/1475-7516/2022/05/013>.
89. Chang, Z.; Zhang, X.; Zhou, J.Z. Primordial black holes and third order scalar induced gravitational waves. *arXiv* **2022**, arXiv:2209.12404.
90. Chen, C.; Ota, A.; Zhu, H.Y.; Zhu, Y. Missing one-loop contributions in secondary gravitational waves. *arXiv* **2022**, arXiv:2210.17176.
91. Meng, D.S.; Yuan, C.; Huang, Q.G. One-loop correction to the enhanced curvature perturbation with local-type non-Gaussianity for the formation of primordial black holes. *Phys. Rev. D* **2022**, *106*, 063508. <https://doi.org/10.1103/PhysRevD.106.063508>.

Disclaimer/Publisher's Note: The statements, opinions and data contained in all publications are solely those of the individual author(s) and contributor(s) and not of MDPI and/or the editor(s). MDPI and/or the editor(s) disclaim responsibility for any injury to people or property resulting from any ideas, methods, instructions or products referred to in the content.